RSC Advances

PAPER

View Article Online
View Journal | View Issue

Cite this: *RSC Adv.*, 2025, **15**, 42479

Evaluation of *Tamarix Aphylla* extract as an eco-friendly corrosion inhibitor for carbon steel in saline medium

Salima Lahbabi, *[a] Rachid Bouferra,[b] Latifa Saadi[a] and Aziza Khalil[a]

The concentration effect of *Tamarix Aphylla* (TA) extract was investigated as a green corrosion inhibitor for carbon steel (E24) in saline solution. The extract was obtained by the maceration method using ethanol solution. Subsequently, the composition of the TA extract was characterized through a combination of phytochemical analysis, Fourier Transform Infrared Spectrometer (FTIR), and High-Performance Liquid Chromatography (HPLC). The TA extract was found to be rich in polyphenols (582.5 mg GAE per g of dry weight), with vanillic and *para*-coumaric acids as the primary polyphenolic compounds. Additionally, the extract demonstrated strong antioxidant activity, with an IC_{50} value of 5.33 mg mL^{-1}. These results suggest that TA could be an effective corrosion inhibitor. For this reason, it was tested as an eco-friendly corrosion inhibitor for E24. Corrosion inhibition performance was assessed using several electrochemical techniques: open circuit potential (OCP), electrochemical impedance spectroscopy (EIS), and potentiodynamic polarization (Tafel) measurements to determine the optimal inhibitor concentration for minimising the corrosion rate of steel. The morphology of the steel surface was analyzed using scanning electron microscopy (SEM). The results indicated that the TA extract, at an optimal concentration of 50 ppm, provides excellent corrosion protection in saline solution (~98% inhibition according to Tafel and ~80% according to EIS). TA acted as an anodic inhibitor. In this study, the extract effectively formed a protective film on the steel surface, enhancing its resistance to corrosion. At higher concentrations, the protective efficiency decreased, likely due to heterogeneous film formation, as shown by SEM-EDX analyses. TA adsorption followed the Langmuir isotherm. Thermodynamic and electrochemical data suggest mainly physisorption. The corrosion inhibition mechanism was shown to be strongly dependent on the extract concentration, and a comprehensive explanation is provided below, suggesting a potential for practical application in corrosion prevention.

Received 12th September 2025
Accepted 22nd October 2025

DOI: 10.1039/d5ra06912b

rsc.li/rsc-advances

1 Introduction

Carbon steel is of crucial importance in numerous industrial sectors, including construction, transportation, manufacturing, and aerospace, due to its excellent mechanical and structural properties, wide availability, and low cost.[1,2] Notwithstanding these advantages, carbon steel is highly vulnerable to corrosion when exposed to aggressive environments, such as humid atmospheres and soils, or saline or fresh water.[3] Continuous exposure to such conditions over an extended period can lead to a significant degradation of the material's integrity, resulting in economic losses and safety concerns.

Corrosion represents a substantial threat to the durability of industrial structures and equipment. According to ISO 8044, corrosion is defined as a process that degrades metals as a result of their interaction with their surrounding environment.[4] This phenomenon has the potential to exert adverse effects on the performance and lifespan of metal structures.[5]

The process of corrosion mitigation using corrosion inhibitors is both straightforward and cost-effective.[3] Corrosion inhibitors, whether organic or inorganic, are chemical compounds added in small quantities to liquid or gaseous media to reduce or prevent the occurrence of corrosion.[6] These chemical inhibitors are considered toxic for the environment, hence the need to move towards a more sustainable and eco-responsible approach.[7,8] In the field of carbon steel corrosion control, research is being actively pursued to develop more effective and environmentally friendly protection strategies for industry and research communities.[9–23] Naturally occurring corrosion inhibitors often demonstrate superior performance compared to conventional options, which frequently consist of toxic organic and inorganic substances.

[a]*Laboratory of Innovative Materials, Energy and Sustainable Development, Chemistry Department. Faculty of Sciences and Technology, Cadi-Ayyad University, B.P. 549, Marrakech, 40000, Morocco. E-mail: salima.lahbabi1@gmail.com; s.lahbabi.ced@uca.ac.ma*

[b]*Laboratory of Geosciences, Geoenvironment and Civil Engineering, Civil Engineering Department. Faculty of Sciences and Technology, Cadi-Ayyad University, B.P. 549, Marrakech, 40000, Morocco*

The use of natural corrosion inhibitors can be traced back to the 1930s, when plant extracts, notably *Chelidonium majus* (dried stems, seeds, and leaves), were evaluated in sulfuric acid pickling solutions.[24] In 1964, tannins and their derivatives were employed in the protection of steel, iron, and various metal tools.[25] The development was further advanced by Marangoni and Stephanel, who in 1972 reported on the effectiveness of glue, gelatin, and wheat extracts in inhibiting iron corrosion in acidic environments.[25]

Natural inhibitors are distinguished by their effectiveness in preventing corrosion and their minimal impact on the environment.[26] A significant number of botanical sources, which are abundant in compounds such as polyphenols, terpenes, alkaloids, and flavonoids, satisfy the criteria of natural and effective inhibitors.[7,27] The employment of natural products, including but not limited to sugarcane bagasse,[27] coconut coir dust,[21] green tea,[28] rape grist (*Brassica napus*),[23] olive leaves,[13] feverfew root,[16] prickly pear seed oil,[17] rice husk ash,[27] green *Bambusa Arundinacea* leaves,[29] ginger,[8] and *Ricinus communis*,[30] is currently under consideration for its potential to delay the onset of corrosion.

Plants offer a multitude of potential sources of inhibitors, from leaves to roots, fruits, flowers, oil, the entire plant, and woody parts (stems, branches, and bark), as well as plant waste. Each of these elements contains a variety of compounds with inhibitory properties and different levels of efficacy. The majority of research has been concentrated on widely available species. *Tamarix Aphylla* is a shrub that grows to be 2 to 5 meters tall and has evergreen, needle-like leaves. It grows along the edges of valleys in semi-arid and dry regions, particularly in North, East, and Central Africa, as well as parts of the Middle East, West Asia, and South Asia. Its leaves are available year-round. This shrub has been used for pharmaceutical purposes for its antidiarrheal, antipyretic, analgesic, antirheumatic, and anti-inflammatory properties.[31] In contrast, the present study explores the inhibitory potential of *Tamarix Aphylla* leaves for the first time, an abundant and undervalued biomass in the Al Haouz region (Tamazouzte, Morocco). A field survey conducted among local residents by authors in a previous study[32] revealed that this shrub grows spontaneously in the region, is not used locally, and is often uprooted to clear agricultural land, although it regrows quickly after removal. This natural and unexploited availability makes *Tamarix Aphylla* a local resource with high potential for development in terms of sustainable development and the circular economy. Unlike previous studies on the bark of *Tamarix Aphylla* from Saudi Arabia by Ismat H. Ali,[33] the *Tamarix Aphylla* leaves have, to the best of our knowledge, not previously been investigated for corrosion inhibition. In this study, *Tamarix Aphylla* leaves extract (TA) was employed as an eco-friendly inhibitor for E24 carbon steel in a 3% NaCl solution. A comprehensive investigation has been conducted into the corrosion inhibition efficiency of TA on carbon steel, using different electrochemical techniques, various adsorption isotherm models, and an examination of the impact of concentration on surface protection. Furthermore, surface analyses by scanning electron microscopy (SEM) coupled with energy-dispersive X-ray spectroscopy (EDX) were performed to further elucidate the morphology and elemental composition of the steel surface after exposure, providing deeper insight into the inhibitory action of the TA extract. These aspects clearly underline the scientific novelty and original contribution of the present study.

2 Materials and methods

2.1 Preparation and characterisation of *Tamarix Aphylla* extract

The leaves of *Tamarix Aphylla* (TA) were collected near the Ourika valley (31°19′32.009″ North and 7°56′39.994″ West), at Tamazouzte, Al Haouz region. The leaves were then washed to remove dust, dried, and ground using a stainless steel blade chopper. Subsequently, the samples were then sieved through a 400 μm sieve and preserved in storage boxes under laboratory conditions. In the present study, the inhibitor was prepared as follows: a quantity of 10 grams of ground TA leaves was mixed with 100 mL of absolute ethanol. The mixture was then stirred for 72 hours at room temperature. The resulting extract was vacuum filtered and oven-dried at a low temperature (40 °C) to produce the corrosion-inhibiting powder, which was then stored in a closed container under laboratory conditions. The schematic diagram illustrating the extraction of TA is presented in Fig. 1.

The obtained powder was characterized by Fourier-transform infrared spectroscopy (FTIR) to analyze the chemical bonds and structural properties. Moreover, the determination of total polyphenolic content, total flavonoid content, and DPPH radical scavenging activity in the corrosion inhibitor was carried out according to the following protocols:

2.1.1 Polyphenolic content. The determination of phenolic compounds was carried out using the Folin–Ciocalteu reagent. First, an aliquot of the sample (0.25 mL) was mixed with 0.15

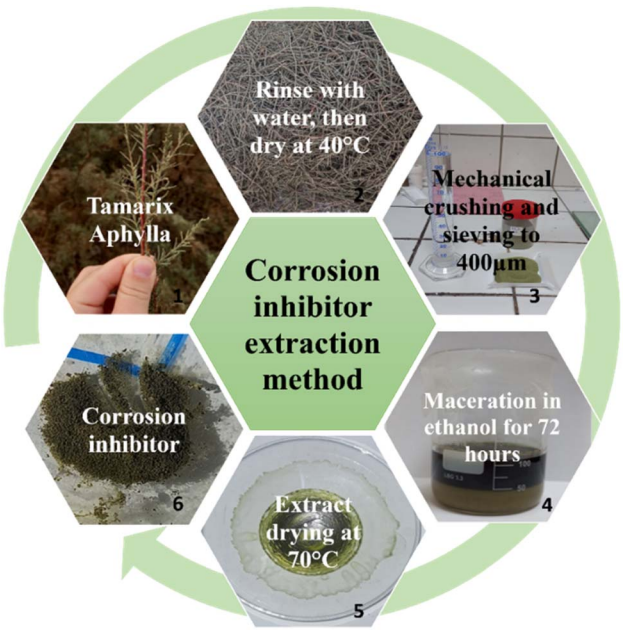

Fig. 1 Corrosion inhibitor extraction process.

mL of the reagent and 1 mL of a 15% sodium carbonate solution. Then, distilled water was added to bring the final volume to 2.5 mL. After incubating the mixture for three minutes at 37 °C in a water bath, the absorbance was measured at 750 nm. Gallic acid (Sigma-Aldrich) was employed as the standard, and the results were expressed as micrograms per milliliter of gallic acid equivalents (GAE).

2.1.2 Total flavonoid content. The quantification of total flavonoid content in the plant extract was conducted in accordance with the protocol described by Gul *et al.*.[34] During the six-minute incubation period, 0.5 mL of the extract was mixed with 2 mL of distilled water and 0.15 mL of a 5% $NaNO_2$ solution. Then, 0.15 mL of a 10% $AlCl_3$ solution was added to the mixture and incubated for an additional 6 minutes. The mixture was brought to a total volume of 5 mL by adding a 4% NaOH solution, which was then mixed well. After 15 minutes of incubation, the reaction mixture's absorption was measured at 510 nm. A calibration curve was established using quercetin (Sigma-Aldrich), and the results were expressed as milligrams of quercetin equivalents (QE) per gram of dry weight.

2.1.3 Antioxidant activity. The 2,2-diphenyl-1-picrylhydrazyl (DPPH) test is a common method used to evaluate the antioxidant activity of plant extracts. The quantification of the DPPH radical scavenging capacity was conducted in accordance with the protocol described by Said *et al.*.[35] First, 2 mL of leaf extract were mixed with 1 mL of an ethanolic DPPH solution containing 7.8 mg of DPPH in 100 mL of ethanol. The mixture was vigorously agitated, then left in the dark for a period of 30 minutes at room temperature. Thereafter, the antioxidant activity was measured by determining the decrease in absorption at 517 nm using a UV-visible spectrophotometer. The antioxidant capacity was evaluated by calculating the IC_{50} value (μg mL^{-1}), and the percentage of inhibition was estimated using the following equation:

$$\text{DPPH inhibition}(\%) = \frac{[A_0 - A_1]}{A_0} \times 100 \quad (1)$$

where A_0 is the absorbance of the control test and A_1 is the absorbance of the sample extract after 30 minutes.

2.1.4 FTIR, UV, pH, and HPLC characterization. Phytochemical tests were performed using a Shimadzu UV-2600 spectrophotometer equipped with a dual-beam photometric system. UV-visible absorption spectra were obtained using a wavelength scan ranging from 400 to 800 nm with a precision and increment of 0.1 nm in quartz cuvettes (QS quality, 1 cm × 1 cm × 4 cm^3). This enabled the calculation of the polyphenol and flavonoid content of the plant extract.

The analysis of TA extract powder using FTIR was conducted with a Bruker Vertex 70 spectrophotometer in transmission mode. The pellets were elaborated by mixing 1 mg of sample powder with 99 mg of potassium bromide (KBr), and the analysis covered the spectral range of 400–4000 cm^{-1}. The measurement included 32 scans with a resolution of 4 cm^{-1}.

The phenolic compounds present in the extract were identified and quantified using a high-performance liquid chromatography (HPLC-KNAUER) equipped with a pump (K-1001) and a UV detector that operated at a wavelength of 280 nm. A 5 mL volume of the extract was injected onto a C18 column (Eurospher II 100-5). The flow rate was maintained at 1 mL min^{-1}, and the column temperature was set at 25 °C. The mobile phase consisted of 0.1% formic acid and methanol, with a total runtime of 30 minutes.

The pH measurements are performed on the 3% NaCl solution with different concentrations of TA inhibitor. The pH meter employed in this study is a SevenDirect SD20 from Mettler Toledo.

2.2 Preparation of steel samples

The material used in this work is an E24 carbon steel, which has been precisely cut into dimensions of 3 × 3 × 0.5 cm^3. The E24 steel conforms to the European standard EN 10025-2:2019[36] (formerly known as S235JR). The specimens were obtained from a local mechanical workshop in Morocco, where this steel grade is commonly used for machining and fabrication purposes. The minimum yield strength of the material is approximately 235 MPa. Additionally, E24 steel has a density of 7.8 g cm^{-3}, and a chemical composition that includes 0.60% Si, 0.14% Cu, 0.12% Cr, 0.11% C, 0.1% Ni, 0.02% Mo, and predominantly iron (Fe),[2] with an exposed surface area of 2.5 cm^2. The steel samples were mechanically polished using SiC abrasive papers with grit sizes ranging from 80 to 2000 grit size until achieving a mirror finish. Subsequently, the steel samples were rinsed with distilled water, cleaned with acetone, and dried with cold air.

2.3 Surface characterization

The morphology and chemical elements contents were examined by a scanning electron microscope (SEM, VEGA 3-Tescan), coupled with an energy dispersive X-ray analysis spectrometer (EDAX).

2.3.1 Electrochemical techniques. Electrochemical tests were carried out at a constant room temperature (24 °C), without stirring, within a Teflon electrochemical cell. The latter is equipped with a conventional three-electrode setup: an Ag/AgCl reference electrode (E = 0.199 V) saturated with KCl; a mild steel working electrode (E24); and a platinum counter electrode. The measurements were conducted using a Biologic SP150 galvanostat potentiostat, which was controlled by EC-Lab analysis software. A solution of 70 mL of NaCl (3%) was used as the reference electrolyte, in which several concentrations of TA extract were examined. The experimental procedure entailed a specific sequence of electrochemical measurements. Initially, the open circuit potential (OCP) was recorded. Subsequently, electrochemical impedance spectroscopy (EIS) was performed after 30 minutes of immersion, encompassing a frequency range from 100 kHz to 10 mHz with an amplitude of 10 mV. Finally, polarization curves were measured at a scan rate of 1 mV s^{-1} after one hour of immersion. The electrochemical data obtained were analyzed and fitted using EcLab software. Corrosion current density (i_{corr}) and corrosion potential (E_{corr}) were extracted by linear proportion extrapolation.

The inhibition efficiency (IE%) obtained from the charge-transfer resistance is calculated as follows:

$$\text{IE}(\%) = \frac{R'_{ct} - R_{ct}}{R'_{ct}} \times 100 \quad (2)$$

where: R_{ct} and $R'c_t$ are the charge transfer resistance values in the absence and the presence of inhibitor, respectively.

In the case of the polarisation technique, the inhibition efficiency (IE%) of TA extract on steel was subsequently determined using the following relationship:

$$\mathrm{IE}(\%) = \frac{I_0 - I_{\mathrm{inh}}}{I_0} \times 100 \quad (3)$$

where: I_0 and I_{inh} are the uninhibited and inhibited corrosion current densities, respectively.

The surface coverage (θ) was estimated using the following equation:

$$\theta(\%) = \frac{I_0 - I_{\mathrm{inh}}}{I_0} \quad (4)$$

The standard free energy adsorption (ΔG_{ads}) was calculated using the following equation:

$$\Delta G^{\circ}_{\mathrm{ads}} = -RT\ln(55.5 \times K_{\mathrm{ads}}) \quad (5)$$

where R is the universal gas constant (8.314 J mol^{-1} K^{-1}), T is the absolute temperature (298 K), K_{ads} is the adsorption equilibrium constant, and 55.5 is the molar concentration of water in the solution.

The eqn (6)–(8) show the isotherm models of Langmuir, Freundlich, and Temkin, respectively.

$$\text{Langmuir isotherm}: \frac{C}{\theta} = \frac{1}{K_{\mathrm{ads}}} + C \quad (6)$$

$$\text{Freundlich isotherm}: \ln(\theta) = \ln(K_{\mathrm{ads}}) + n\ln(C) \quad (7)$$

$$\text{Temkin isotherm}: Ln\left(\frac{\theta}{C}\right) = Ln(K_{\mathrm{ads}}) + a\theta \quad (8)$$

3 Results and discussion

3.1 Characterization of TA extract

3.1.1 Total polyphenolic and flavonoid content in TA extract. A review of the relevant literature reveals that phytochemical studies conducted on *Tamarix* species reveals that the primary chemical constituents are polyphenolic compounds, including flavonoids, tannins, and phenolic acids.[37] The total phenolic content of the TA extract was expressed as GAE using the gallic acid calibration curve shown in Fig. 2(a). The findings suggest that TA extract possesses a remarkably high polyphenol concentration, measuring 582.5 mg GAE per g of dry weight. According to the literature, as posited by Mahfoudhi *et al.*,[38] an analysis of *Tamarix Aphylla* leaves yielded a concentration of 993.1 μg g^{-1} of dry weight. Similarly, Gul *et al.*[34] found a concentration of 220.6 mg g^{-1} of EAG/100 g of dry weight. Said *et al.*[35] have also carried out studies on species of the *Tamarix* family, showing phenolic compound content of 395.62 and 334.19 mg GAE per g dry weight in *Tamarix articulata* and *Tamarix gallica*, respectively.

The total flavonoid content is calculated using the regression equation from the quercetin standard calibration range, as shown in Fig. 2(b). The total flavonoid content of the TA extract is 2.90 mg QE per g of dry plant extract. This value is close to the one reported by Ksouri *et al.*,[39] which is approximately 3.91 mg QE per g of dry *Tamarix gallica* leaf extract.

3.1.2 Antioxidant activity: DPPH radical scavenging activity. The DPPH free radical is widely considered as a stable organic free radical and is commonly accepted as a method for evaluating the free radical scavenging capacity of antioxidants.[35,40] The DPPH test showed that the TA extract has significant antioxidant activity, with an IC_{50} of 5.33 mg mL^{-1} (Fig. 3). The findings indicate that a concentration of 5.33 mg mL^{-1} is sufficient to scavenge 50% of DPPH free radicals. These results are consistent with the findings reported by Said *et al.*,[35] who demonstrated that other species of the *Tamarix* family exhibit high concentrations of DPPH radicals. Furthermore, as illustrated in Fig. 3(b), the extract exhibits significant inhibition at low concentrations, but this activity diminishes as the TA extract concentration rises.

3.1.3 Fourier transform infrared spectroscopy of TA. The primary chemical components in the TA extract were identified through the implementation of Fourier-transform infrared (FTIR) analysis. Fig. 4 shows the FTIR spectrum of TA, which manifests several transmittance bands. The presence of a broad band at 3356 cm^{-1} is indicative of hydroxyl (OH) groups in

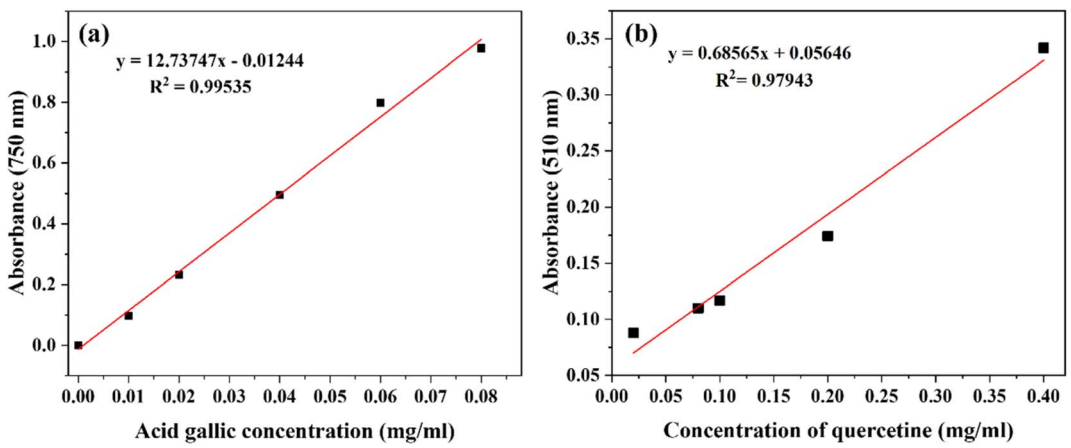

Fig. 2 Calibration curves for (a) polyphenols and (b) flavonoids.

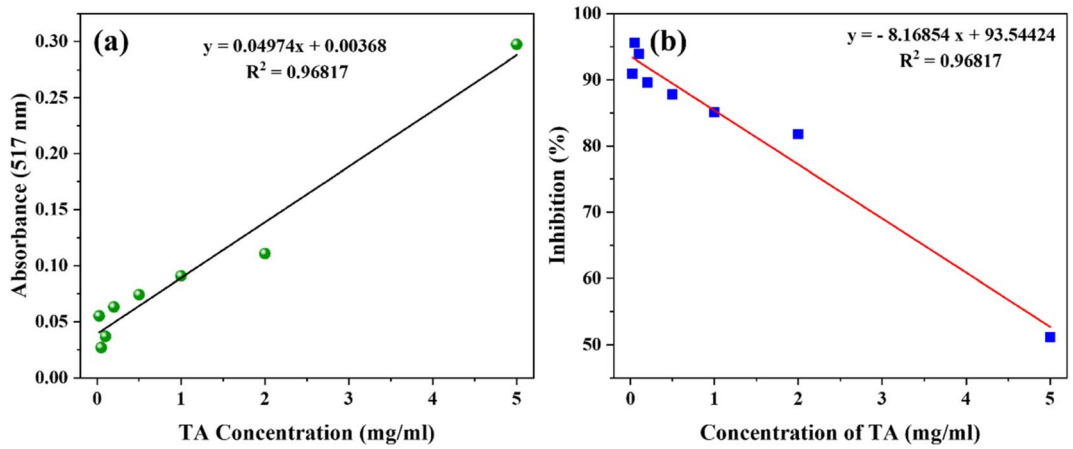

Fig. 3 (a) The DPPH free radical calibration curve, and (b) the percentage of DPPH inhibition as a function of different TA concentrations.

phenolic or alcoholic compounds.[19,41] Peaks at 2923 and 2851 cm^{-1} correspond to the stretching vibrations of saturated hydrocarbons (Csp^3-H)[19,42,43] and the C–H stretching of the CH_2 alkane,[19,41] respectively. The bands at 1729 and 1614 cm^{-1} correspond to the C═O stretching of the carbonyl group,[41–43] and the peak at 1515 cm^{-1} is attributed to the N–H torsion and C–N stretching bonds of amide.[19] The band at 1448 cm^{-1} can be assigned to the aromatic ring (C═C) vibrations,[42] and the band at 1348 cm^{-1} corresponds to the $-CH_3$ stretching vibrations.[43] The transmittance bands between 1300 and 1000 cm^{-1} are consistent with the C–OH stretching vibrations in alcohols, carboxylic acids, and esters.[19,41,42] The low-wavelength region between 400 and 1000 cm^{-1} is characteristic of the extract's fingerprint. The band at 757 cm^{-1} is attributed to CH_2 oscillation,[19] and the bands at 644 and 597 cm^{-1} correspond to C–H vibration of the aliphatic or aromatic group.[43] These observations are consistent with phytochemical tests showing a high concentration of polyphenols.

3.1.4 HPLC analysis. High-performance liquid chromatography (HPLC) is the most common technique used to analyse phenolic acids and flavonoids in plant extracts. The identification of HPLC peaks is achieved through a comparison of their retention times to those in the literature. Fig. 5 shows the HPLC chromatogram of TA leaves extract.

The TA extract contains several phenolic compounds, including vanillic acid, paracoumaric acid, epicatechin, gallic acid, syringic acid, rosmarinic acid, caffeic acid, and ferulic acid. These polyphenols are well-known phenolic acids that are widely present in the *Tamarix* family.[35,38,39,42] Additionally, the extract contains flavonoids, such as quercetin, a famous flavonoid detected in several *Tamarix* species,[37] and flavone.[39,42] The peaks for vanillic and paracoumaric acids are the most intense, explaining their high concentration in the extract. Similarly, Gul *et al.*[34] reported the presence of high concentrations of these phenolic compounds in *Tamarix Aphylla* leaf extract, measuring at 45.59 ppm for quercetin and 32.38 ppm for flavone. Said *et al.*[35] also found that *Tamarix gallica* and *articulata* extracts are both rich in vanillic acid.

The compounds detected in the extract following HPLC analysis are presented in Fig. 6. The HPLC results are in line

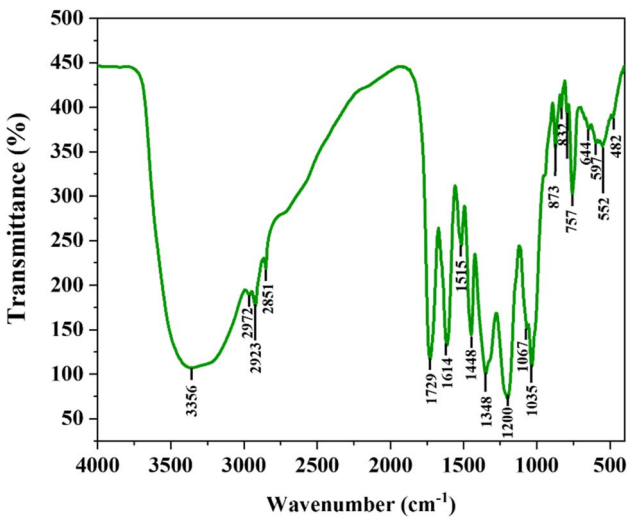

Fig. 4 FTIR spectra of TA extract.

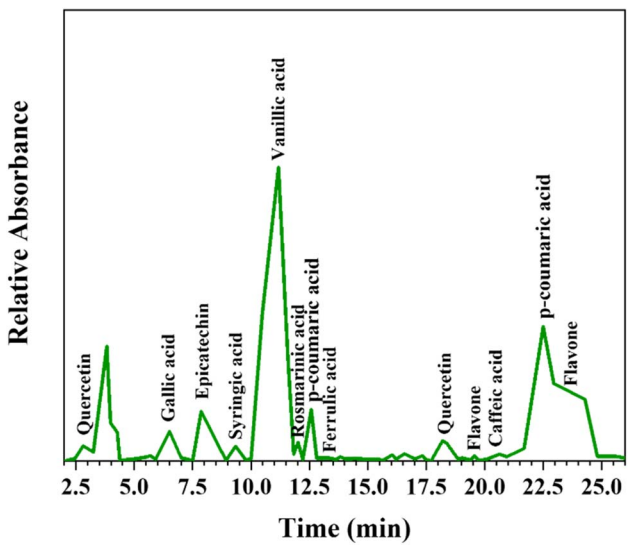

Fig. 5 HPLC chromatogram of ethanolic leaves extract from TA.

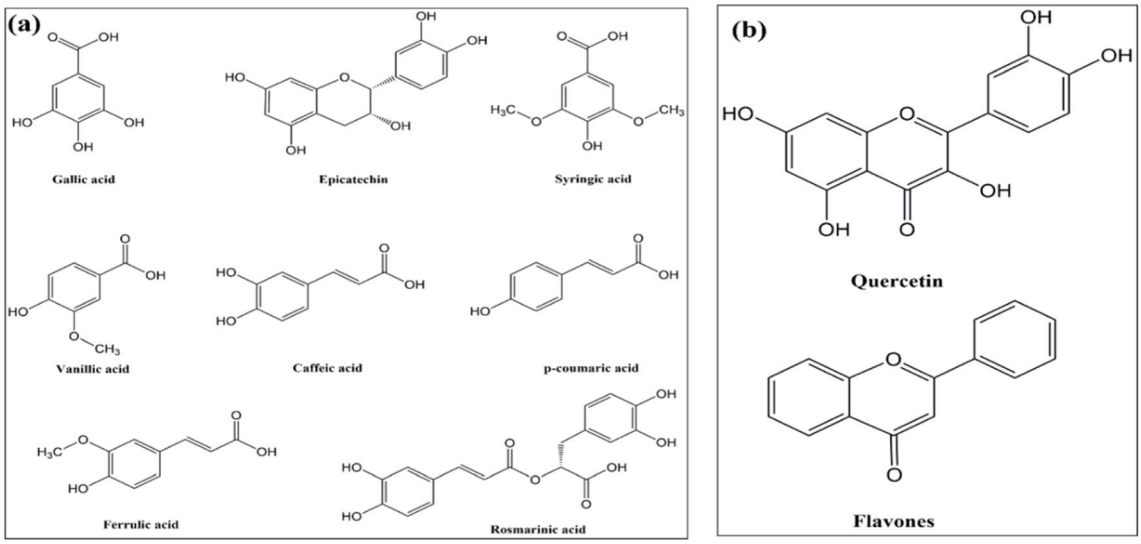

Fig. 6 Different (a) polyphenols and (b) flavonoids present in TA extract.

with those from FTIR analysis and phytochemical tests, showing that the various compounds are acids with aromatic rings.

3.1.5 Synopsis of the TA extract characterization. The phytochemical analysis of the TA extract indicated the presence of polyphenols and flavonoids. This result was confirmed by the presence of various aromatic rings, as indicated by FTIR analysis. Furthermore, the outcomes of the antioxidant activity assay demonstrated that TA extract exhibited a notably high level of activity even at low concentrations. The results of the present study align closely with extant literature on *Tamarix* species, which consistently indicates a high content of phenolic compounds. These compounds are well-known for their antioxidant properties.[35,44,45] Moreover, Younos *et al.*[44] reported that *Tamarix* species are abundant in phenolic compounds, which have been implicated in a variety of biological activities, including antioxidant properties. In addition, the high-performance liquid chromatography results indicated higher phenolic compositions in the extract, thereby suggesting that the observed high antioxidant capacity could be primarily attributed to the presence of polyphenols.

The diversity of phenolic compounds in the extract, as evidenced by the various characterization studies, suggests a promising potential for its use as a corrosion inhibitor.

3.2 Effect of TA concentration on solution pH

To evaluate the effect of TA extract on the pH of the corrosive medium, pH measurements were performed for different inhibitor concentrations in 3% NaCl solution. The results presented in Table 1, show a progressive decrease in pH with increasing TA concentration, indicating a shift toward more acidic conditions. This behavior is expected, as the extract is predominantly composed of various organic acids, including vanillic acid, as confirmed by HPLC-UV analysis, and its initial pH was measured at 3.98.

Table 1 pH measurements of different TA inhibitor concentrations in 3% NaCl

	NaCl 3%	10 ppm TA	50 ppm TA	100 ppm TA	1 g L^{-1} TA	2 g L^{-1} TA
pH	5.95	5.61	5.50	5.35	4.69	4.61

3.3 Electrochemical behavior at corrosion potential

Prior to conducting a detailed examination of the corrosion behavior of E24 steel in a corrosive environment, it is worthwhile to observe the evolution of the free potential (OCP) as a function of time in the presence and absence of a TA inhibitor, as illustrated in Fig. 7. The corrosion potential values in the absence and presence of TA are of the same order of magnitude, ranging from −0.616 to −0.694 V. The presence of TA extract

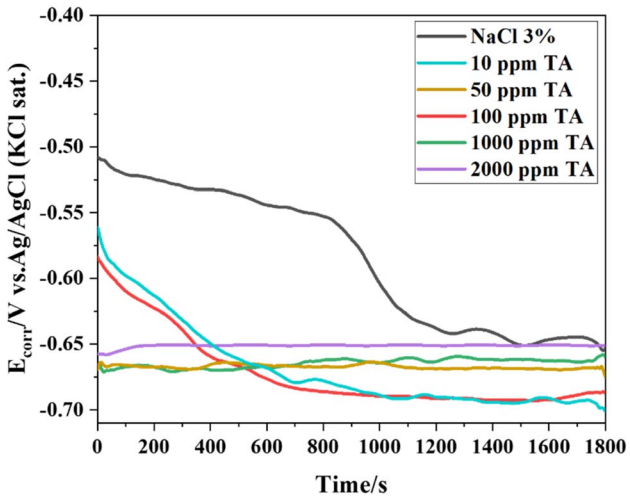

Fig. 7 Free potential monitoring of E24 steel in a 3% NaCl medium in the presence of different concentrations of TA.

induces a cathodic shift in the corrosion potential. This shift was also observed by Yamamoto *et al.*,[46] who found that the inhibition of pure iron in 0.5 M NaCl solutions by sodium 3-*n*-octylmercaptopropionate resulted in pitting caused by local ruptures of the protective film on the electrode surface. These ruptures, which are caused by the aggressive nature of the medium, generate dissolution sites that make the potential more negative. However, the inhibitor has been shown to rapidly repair these ruptures by forming a protective film, thereby restoring the corrosion potential to more noble and stable levels.

3.4 Electrochemical impedance spectroscopy

Fig. 8 presents the electrochemical impedance spectroscopy (EIS) plots illustrating the corrosion process of E24 steel in the presence of different concentrations of TA extract in 3% NaCl. The Nyquist diagrams illustrate a single capacitive loop that increases with the TA extract concentration up to 50 ppm, then decreases for higher concentrations: the metal exhibits reduced corrosion resistance. However, Fig. 9 shows the Bode diagrams of E24 carbon steel immersed in a 3 wt% NaCl solution with and without different concentrations of TA extract. The modulus impedance (Fig. 9(a)) increases with the TA concentration until it reaches 50 ppm of TA, after which a decrease is observed. In contrast, the phase angle provides insight into the balance of capacitive and resistive behaviors at the electrochemical interface.[47] Higher phase angles approaching 60° at intermediate frequencies, which is less than the ideal 90°, indicate that the inhibitor film exhibits characteristics of a non-ideal capacitor.[47,48] This suggests the formation of a protective yet heterogeneous layer on the steel surface in the presence of TA that hinders the ingress of aggressive chloride ions. This film restricts charge transfer across the interface, consequently reducing the corrosion rate. The Bode diagrams confirm the presence of a single time constant, which is characteristic of charge-transfer controlled corrosion processes in the studied medium.

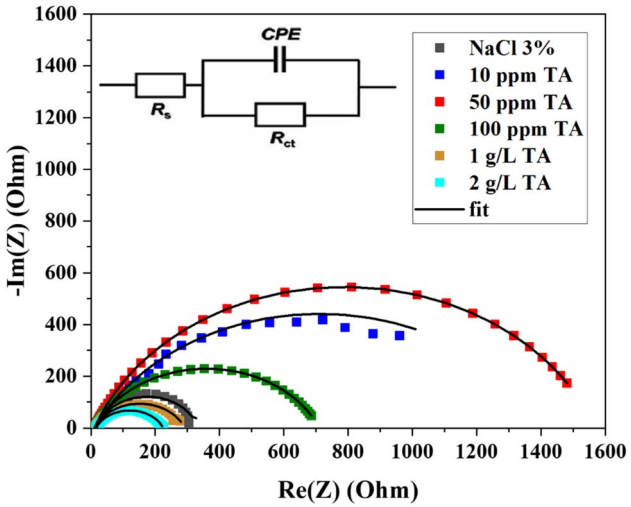

Fig. 8 Nyquist diagram of E24 steel in NaCl 3% at different concentrations of TA extract.

The equivalent electrical circuit (EEC), likely to reflect the behavior of the metal/solution interface, is a Randles circuit. The latter consists of the electrolyte resistance (R_s), which is connected in series with the charge transfer resistance (R_{ct}) in parallel with a double-layer capacitor (Q_{dl}), as shown in Fig. 8. This modelling led to the electrochemical corrosion parameters of E24 steel in a 3% NaCl solution with and without TA inhibitor at various concentrations. The electrochemical parameters obtained from fitting the EEC, along with the corresponding inhibition efficiencies, are listed in Table 2.

The charge transfer resistance is correlated with the impedance modulus at a low frequency $|Z|_{0.01}$ Hz. For the uninhibited solution, it was 316.1 Ω cm^2 at 10 mHz, whereas

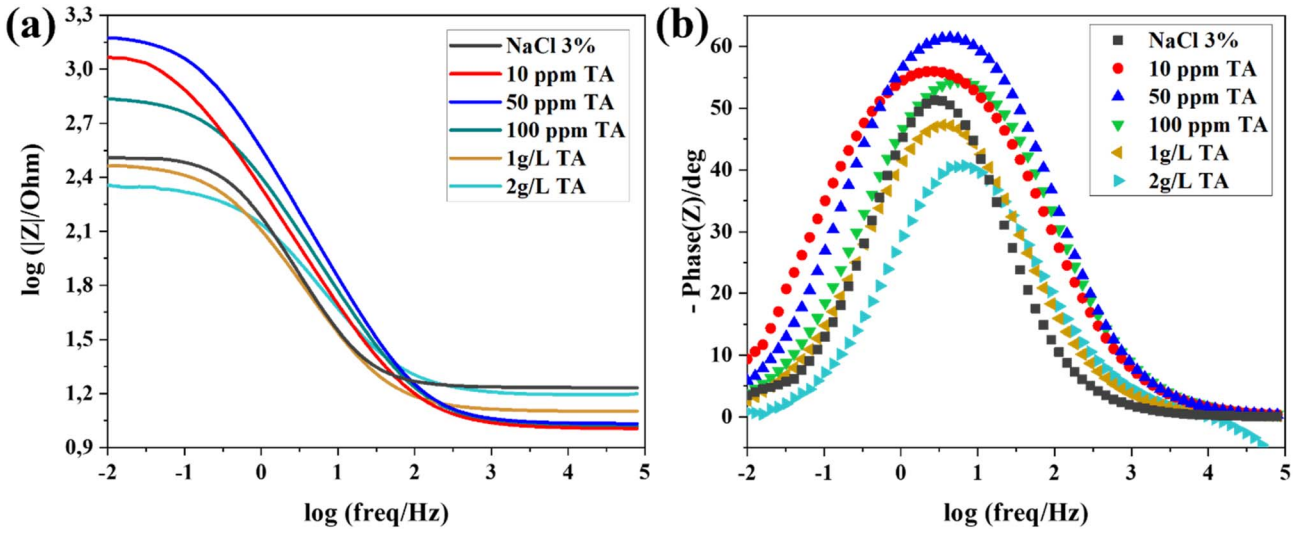

Fig. 9 Bode diagrams illustrating the effect of TA concentration on the corrosion of E24 steel in 3% NaCl solution: (a) impedance modulus and (b) phase angle.

Table 2 The electrical parameters and corrosion-inhibiting efficiencies of E24 steel in NaCl 3% in the absence and presence of different concentrations of TA

	R_s (Ω cm^2)	Q_{dl} (mF s^{-n})	n	R_{ct} (Ω cm^2)	IE$_{R_{ct}}$ (%)
NaCl 3%	17.08	1.36	0.80	316.1	—
10 ppm TA	10.09	1.23	0.70	1402	77.45
50 ppm TA	10.75	0.62	0.77	1557	79.70
100 ppm TA	10.39	0.85	0.74	699.4	54.80
1 g L^{-1} TA	12.63	1.23	0.76	278.6	—
2 g L^{-1} TA	15.57	0.74	0.73	209.3	—

adding 50 ppm TA increased this value to 1557 Ω cm^2, indicating the optimal concentration for corrosion protection. The increase in R_{ct} can be associated with the adsorbed TA molecules forming a stable layer[2] on the steel surface, which limits the dissolution of E24 carbon steel. Beyond this concentration, a slight decrease was observed. The increase in R_{ct} and inhibition efficiency confirms the formation of this adsorbed film.

The inhibitory efficiency increases with lower concentrations of TA inhibitor, reaching 80% at 50 ppm TA. At concentrations exceeding this level, inhibitory efficiency gradually declines, reaching 55% at 100 ppm TA. However, at higher concentrations, the inhibitor has been observed to accelerate the corrosion process. This phenomenon occurs when the concentration of TA extract exceeds roughly 50 ppm. Furthermore, the tests revealed that a TA concentration above of 1 g L^{-1} had a deleterious effect on the material, significantly increasing the corrosion rate. At higher concentrations, the steel surface becomes saturated,[20] preventing the formation of a continuous and compact protective film. This can leave some areas insufficiently protected, thereby reducing the overall resistance to charge transfer, which reduces the effectiveness of corrosion inhibition. A similar electrochemical trend was reported by Juarez *et al.*,[49] who correlated this behavior to the formation of micelles at the critical micelle concentration (CMC). According to their interpretation, once the CMC is reached, the inhibitor molecules preferentially interact with each other due to their mutual affinities, leading to aggregates or micelle formation rather than further adsorption on the metal surface, which results in a reduction of the inhibition efficiency at higher concentrations.

This phenomenon could be related to factors such as the concentration, steric effects, and critical micelle concentration[49] of the TA extract, as will be discussed in the following section.

Conversely, the capacity of the double layer declines at low concentrations compared to the blank solution. This phenomenon is likely attributable to the displacement of water molecules and the adsorption of the TA inhibitor molecules onto the steel surface.[50] The adsorption process results in either a reduction of the dielectric constant of the medium or an increase in the thickness of the electrical double layer.[51,52] This clearly demonstrates that the TA molecules effectively adsorb onto the metal surface,[53] creating a protective layer that limits the number of active sites available for anodic dissolution and thereby inhibiting the corrosion of E24 steel.

3.5 Potentiodynamic curves

The polarization curves were determined by applying a potential to the E24 steel relative to the Ag/AgCl reference electrode, as illustrated in Fig. 10. The electrochemical parameters derived from the polarization curve, including the corrosion current density (i_{corr}) and the corrosion potential (E_{corr}), are presented in Table 3. In the presence of TA inhibitor, the corrosion potentials shift towards more anodic values, ranging from −812 mV to −681 mV *vs.* Ag/AgCl for 50 ppm TA, compared to the electrode's potential in the absence of inhibitor. The i_{corr} value of the steel samples is observed to be higher in the absence of an inhibitor, with an approximate measurement of 12.72 μA cm^{-2}. The results show that the system containing 50 ppm of TA extract exhibits a corrosion rate that is 47 times lower compared to the control system, which did not contain TA extract. As the TA concentration increases, the corrosion current densities decrease in comparison with those of the blank solution, and an optimum of 98% inhibition efficiency was reached for a TA concentration of 50 ppm. It has been established that an increase in TA concentration (100 ppm, 1 g L^{-1}, and 2 g L^{-1}) resulted in a slight increase in the corrosion rate. This phenomenon can be attributed to the congestion of the solution at high concentrations,[20] which disrupts uniform adsorption on the steel surface, a topic that will be addressed in the following discussion. Additionally, at low concentrations, the cathodic curves remain unaltered, both with and without the inhibitor. It is evident that there is a marginal shift at the highest concentrations, which indicates a predominantly anodic effect, accompanied by a minor cathodic response at these levels. The pronounced modification of the cathodic branch at 2 g L^{-1} may result from partial blocking of oxygen reduction sites by heterogeneous adsorption of TA molecules or from O_2 mass-transport limitation induced by TA aggregate formation, which

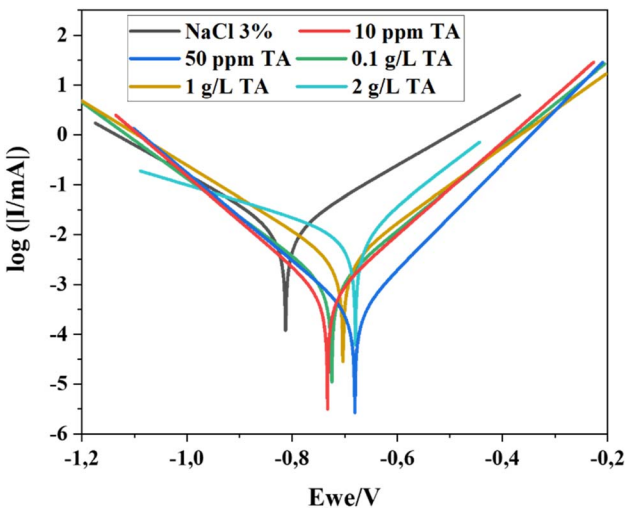

Fig. 10 Polarization curves for E24 steel in 3% NaCl without and with TA at different concentrations.

Table 3 Polarization parameters of E24 steel in NaCl 3% in the absence and presence of different concentrations of TA

Concentrations	NaCl 3%	10 ppm TA	50 ppm TA	100 ppm TA	1 g L^{-1} TA	2 g L^{-1} TA
E_{corr} (mV)	−812	−733	−681	−725	−703	−679
i_{corr} (μA cm^{-2})	12.715	0.581	0.271	1.041	2.914	5.879
IE (%)	—	95.43	97.87	91.81	77.08	53.76
θ	—	0.95	0.98	0.92	0.77	0.54

affect the cathodic reaction kinetics.[54] It can be deduced that TA acts as an anodic inhibitor. Conversely, efficiency decreases when the TA concentration exceeds 50 ppm, indicating the critical concentration. The findings obtained in this study are consistent with those previously reported by EIS.

The inhibition efficiency (IE%) of TA on E24 steel in a 3% NaCl medium was evaluated using two complementary techniques: potentiodynamic polarization and electrochemical impedance spectroscopy (EIS). The results obtained from both methods show a similar trend, with the maximum inhibition efficiency attained at a TA concentration of 50 ppm.

3.6 Adsorption isotherm analysis

Adsorption isotherm models have been proven to be an effective means of investigating the mechanism by which organic molecules adsorb during electrochemical reactions. To understand the adsorption behavior of TA on the steel surface in a chloride solution, adsorption isotherm models were investigated to ascertain the most appropriate model to describe the interaction between the inhibitor molecules and the metal surface. These models were established based on experimental results derived from polarization curves. Adsorption mechanism insights were obtained by fitting the experimentally determined surface coverage (θ) values to three standard adsorption isotherm models: Langmuir, Freundlich, and Temkin. The linear equations for each model were utilized to calculate the model parameters and their respective correlation coefficients (R^2). Among the models that were examined, the Langmuir adsorption isotherm demonstrated the best agreement with the experimental results, as shown in Fig. 11. This model, which describes monolayer adsorption on a uniform surface with no significant interactions between adsorbed species, yielded correlation coefficients ($R^2 = 0.999$) very close to 1. The adsorption equilibrium constant obtained from the Langmuir plot was 77.9 L mol^{-1}. From this value, the standard free energy is −20.8 kJ mol^{-1}. This negative value suggests the spontaneous nature of the adsorption process, as well as the stability of the inhibitor layer on the mild steel surface. The magnitude of the free energy of adsorption, ΔG_{ads}, is indicative of the nature of the adsorption process. This latter can be inferred from the standard free energy of adsorption (ΔG_{ads}). According to the literature, when ΔG_{ads} values are around −40 kJ mol^{-1} or more negative, this suggests the involvement of charge sharing or transfer between the organic molecules and the metal surface, indicating chemisorption.[33,55,56] In contrast, for values less negative than −20 kJ mol^{-1}, the process is generally dominated by electrostatic interactions, corresponding to physical adsorption,[50,57] which appears to be the prevailing mechanism in the present system.

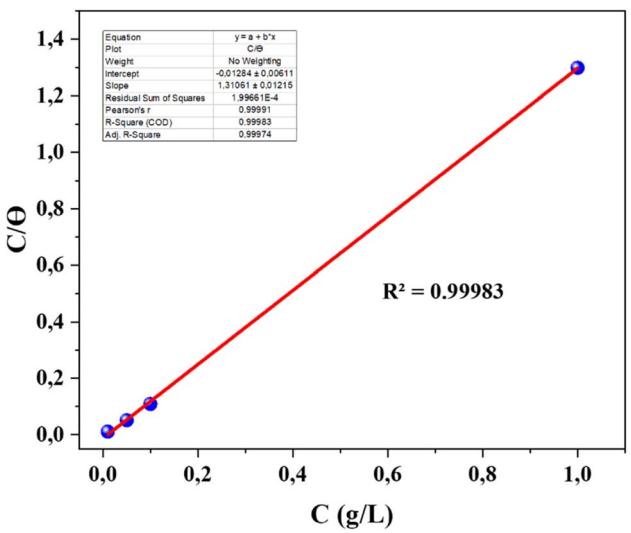

Fig. 11 Langmuir adsorption isotherm of TA on the E24 steel surface in 3% NaCl solution.

3.7 Steel surface analysis

To confirm the results from the electrochemical tests, SEM observations were complemented by quantitative EDX analysis. Scanning electron microscopy analyses were carried out on E24 steel samples that had been previously polished and immersed for 24 hours in a 3% NaCl solution, in the absence and presence of TA inhibitor at different concentrations (Fig. 12).

Fig. 12(a) shows the surface of a freshly polished carbon steel sample before immersion. There is no corrosion present, and the surface appears very smooth. EDX spectra of the control sample (Fig. 12(e)) show that iron and carbon are the main elements present in the sample. The micrograph depicted in Fig. 12(b) reveals an unprotected steel surface that has been extensively corroded, with corrosion products that have spread across the surface of the metal, forming a heterogeneous layer. The EDX spectrum of the sodium chloride solution without an inhibitor (Fig. 12(f)) reveals a high oxygen content in the sample, along with small peaks corresponding to sodium and chloride atoms. This suggests the presence of iron oxides[58] (FeO and Fe_2O_3), iron chloride ($FeCl_2$), and hydroxide species[58] (FeOOH) on the iron surface. Conversely, in 50 ppm TA, the steel surface exhibits a morphology with considerably diminished corrosion products (Fig. 12(c)). Corrosion reduction is associated with forming a protective film on the steel surface.

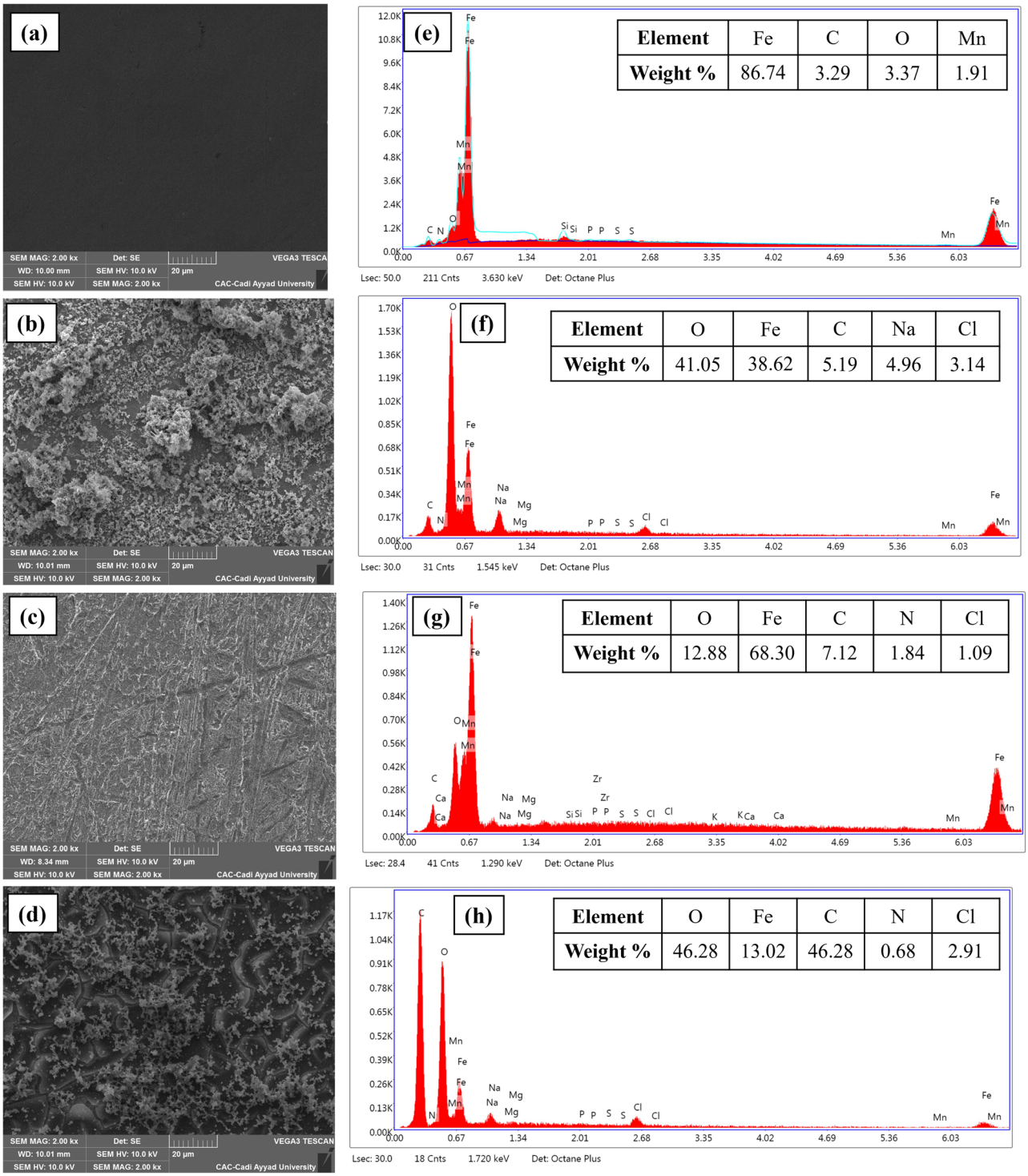

Fig. 12 SEM micrograph and EDX spectra of the surface of E24 steel freshly polished (a and e), after 24 h immersion in a 3% NaCl solution in the absence (b and f), and in the presence of 50 ppm (c and g), and 2 g L^{-1} TA (d and h).

This acts as a barrier, preventing corrosive species from reaching the steel's active sites, as observed in the work of Chowdhury *et al.*.[28] The corresponding EDX spectrum in (Fig. 12(g)) shows a decrease in the oxygen, iron and chloride peaks, disappearance of the sodium peak, and an increase in the carbon peak in the presence of 50 ppm TA. These changes undoubtedly indicate the presence of TA molecules on the iron surface, which block damage and prevent the formation of corrosion compounds thanks to their strong chemical adsorption on the steel surface.

Furthermore, the surface of sample E24 exhibits increased roughness, damage, and cracking in the presence of 2 g L^{-1} TA (Fig. 12(d)). This observation indicates that a high inhibitor content has resulted in a deterioration in the surface condition

relative to the absence of inhibitor. This finding aligns with the observations reported by Zhang *et al.*,[55] who also noted a diminished effectiveness of the inhibitor when its critical concentration is exceeded. Additionally, the SEM image reveals the presence of aggregates. At higher concentrations of the TA inhibitor, the corresponding EDX spectrum (Fig. 12(h)) exhibits increased carbon and oxygen peaks. These observations highlight the presence of iron oxides[58] (FeO and Fe_2O_3), hydroxide species[58] (FeOOH), and TA molecule aggregation on the iron surface. This aggregation induces discontinuities in the protective film, exposing portions of the underlying metal that act as active anodic sites. Such localized exposure can accelerate electrochemical reactions, which may explain the reduction in the protective effect and the corresponding changes in i_{corr} observed at higher concentrations, in agreement with the EIS results.

These microscopic observations confirm the effectiveness of the TA inhibitor optimized at 50 ppm, acting as a protective barrier against corrosion and corroborate the electrochemical tests obtained previously.

3.8 Corrosion inhibition mechanism

The degradation of steel reinforcements in 3% NaCl solution results from an electrochemical mechanism occurring at the steel/solution interface. This process involves the oxidation of the iron component of the steel (eqn (9)) according to an anodic reaction.[6,18]

$$Fe \rightarrow Fe^{2+} + 2e^- \quad (9)$$

To maintain electrical neutrality, the electrons generated by the anodic reaction must be consumed at the cathodic sites on the steel surface. This reaction consists of oxygen reduction[6,18,25] (eqn (10)).

$$\frac{1}{2}O_2 + H_2O + 2e^- \rightarrow 2OH^- \quad (10)$$

The presence of chloride ions Cl^- accelerates the corrosion of the surface of the carbon steel. The following equations show the reaction mechanism of carbon steel in a 3% NaCl solution:

$$NaCl \rightarrow Na^+ + Cl^- \quad (11)$$

$$Fe^{2+} + 2Cl^- \rightarrow FeCl_2 \quad (12)$$

$$FeCl_2 + 2OH^- \rightarrow Fe(OH)_2 + 2Cl^- \quad (13)$$

Fig. 13 illustrates the corrosion inhibition mechanism of *Tamarix Aphylla* extract on E24 mild steel in a 3% NaCl solution. The electrochemical impedance and polarization measurements demonstrate that TA displays remarkable corrosion inhibition performance, primarily by significantly reducing anodic reactions, with its inhibitory effect depending on the TA concentration.

In the presence of low concentrations of TA, the metal is effectively protected. The inhibitor forms a homogeneous protective film on the metal surface, thereby preventing corrosion (Fig. 13(a)). However, at concentrations that exceed a critical limit, the outcomes become more ambiguous and require careful interpretation. The inhibitory efficacy exhibits a substantial decline, attributable to the interplay of multiple factors. A decrease in the corrosion rate is probably due to the formation of a heterogeneous layer on the steel surface. This phenomenon is often the result of the adsorption of corrosion products, TA inhibitor species, or inhibitor-metal complexes on the steel surface.[22] The agglomeration of TA extract molecules (Fig. 13(b)) further exacerbates this phenomenon,[20] delaying the formation of the protective film on the steel surface.

Conversely, an excessive concentration of the inhibitor can generate a counterintuitive effect, as observed in the electrochemical impedance spectroscopy measurements conducted at concentrations of 1 and 2 g L^{-1}. The complexation of iron ions by the inhibitor has been shown to enhance their solubility in the electrolyte. This phenomenon can, paradoxically, accelerate corrosion by increasing the availability of reactive species at the metal surface, thus promoting anodic reactions.[22,59] Furthermore, an excessive complexation of metal ions with TA phenolic groups has been shown to disrupt passive film formation,[60–64] thereby reducing the protection afforded by the inhibitor.

The schematic diagram (Fig. 13(c)) provides a clear illustration of the consequences of an excess of TA inhibitor.

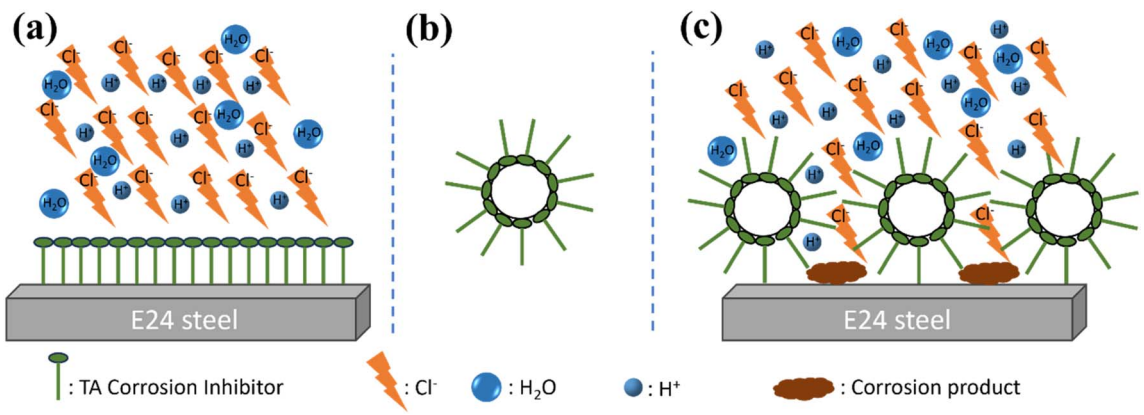

Fig. 13 Representative scheme: (a) metal protection at low TA inhibitor concentrations, (b) congestion of the TA inhibitor molecule at high concentrations, and (c) attack of the steel surface by chlorides at concentrations that exceed the critical level.

Above a certain critical concentration, the disordered adsorption of agglomerated inhibitor molecules creates defects within the protective film, thereby resulting in exposed zones where the metal is susceptible to corrosion. These uncovered regions subsequently become active anode sites, promoting metal oxidation. The anodic sites in question are characterized by a particularly elevated concentration of chloride ions, as demonstrated by EDX analysis (Fig. 12(h)), a factor that has been demonstrated to accelerate the corrosion process. The results of EIS obtained at a concentration of 2 g L^{-1} TA corroborate this trend, with a decrease in charge transfer resistance (R_{ct}).

In summary, it can be concluded that optimum inhibitory efficacy is achieved for a specific concentration. The molecules of the TA inhibitor bind to the metal surface, thereby reducing the available surface area for corrosion reactions.[65] Beyond this limit, the adsorption of inhibitor molecules may reach a level that disrupts the formation of a homogeneous passive film, creating defects that favour anodic reactions.[60,66,67] This behavior is indicative of an adsorptive inhibition process.[65]

4 Conclusion

The present study investigated the effectiveness of *Tamarix Aphylla* (TA) extract as a corrosion inhibitor for E24 steel in 3% NaCl solution. The phytochemical characterization, supported by FTIR and HPLC analyses, revealed that the extract contains a variety of polyphenolic and flavonoid compounds, with particularly high concentration of vanillic and *para*-coumaric acids. Furthermore, the electrochemical tests, including potentiodynamic polarization and EIS which show a similar trend, demonstrated a substantial enhancement in the corrosion resistance of steel in the presence of TA, with optimal inhibition observed at 50 ppm. Additionally, Tafel curves indicated that TA inhibitor acts predominantly as an anodic inhibitor. At higher concentrations, the protective effect was reduced, likely related to the formation of a heterogeneous film on the steel surface. SEM and EDX analyses revealed an irregular surface morphology at 2 g L^{-1}, along with the presence of corrosion products and inhibitor species, suggesting the formation of a non-uniform film.

EIS results revealed slight deviations in inhibition efficiencies compared to polarization data, specifically consistent with the high reliability of the EIS method for corrosion rate evaluation.[68] The adsorption of TA molecules on the steel surface appears to occur mainly through physisorption,[33,56] as supported by the Langmuir model and the calculated ΔG_{ads} (−20.7 kJ mol^{-1}). However, the increase in R_{ct} and the EDX detection of carbon and oxygen peaks indicate localized chemical interactions between the inhibitor and the metal surface. Overall, the inhibition mechanism involves physisorption of TA molecules, resulting in a stable and protective inhibitor layer with long-term efficacy.

Author contributions

Salima Lahbabi: conceptualization, investigation, methodology, visualization, writing – original draft, writing – review & editing. Rachid Bouferra: supervision. Latifa Saadi: supervision. Aziza Khalil: validation, supervision, conceptualization, writing – original draft.

Conflicts of interest

The authors declare that they have no known competing financial interests or personal relationships that could have appeared to influence the work reported in this paper.

Data availability

Data will be made available on request.

Acknowledgements

The authors wish to express their gratitude to the authorities and villagers of Marrakesh – Safi region. The authors would like to thank the institutions that contributed to the realization of this work: Centre d'Analyses et de Caractérisation (CAC) of Cadi Ayyad University, Marrakesh, Morocco, and IMED-Laboratory.

References

1 R. Hsissou, O. Dagdag, S. Abbout, F. Benhiba, M. Berradi, M. El Bouchti, A. Berisha, N. Hajjaji and A. Elharfi, *J. Mol. Liq.*, 2019, **284**, 182–192.
2 N. El-Aouni, O. Dagdag, A. El Amri, H. Kim, R. Haldhar, S. C. Kim, N. Dkhireche, A. El Bachiri, A. Berisha and M. Rafik, *Colloids Surf., A*, 2024, **682**, 132963.
3 M. Damej, S. Skal, J. Aslam, M. Zouarhi, H. Erramli, A. A. Alrashdi, H. S. Lee, Y. El aoufir and H. Lgaz, *Colloids Surf., A*, 2022, **643**, 128745.
4 K. Srivastav and P. Srivastava, *Br. Corros. J.*, 1981, **16**, 221–223.
5 F. Suedile, *Institut d'enseignement supérieure de la Guyane*, 2014.
6 A. Poursaee, *Corrosion of Steel in Concrete Structures*, Woodhead Publishing Series in Civil and Structural Engineering, Elsevier, 2016, vol. 61.
7 P. Bothi Raja and M. G. Sethuraman, *Mater. Lett.*, 2008, **62**, 2977–2979.
8 Y. Liu, Z. Song, W. Wang, L. Jiang, Y. Zhang, M. Guo, F. Song and N. Xu, *J. Clean. Prod.*, 2019, **214**, 298–307.
9 N. Kumar, I. S. Mohd Noor, M. Zu Azhan Yahya and S. Prakash, *Zastita Materijala*, 2024, DOI: 10.62638/zasmat1092.
10 S. H. Fakir, K. Chaitanya Kumar, H. Ali, J. Rawat and I. Haq Farooqi, *Mater. Today Proc.*, 2023, **82**, 29–37.
11 H. Wei, B. Heidarshenas, L. Zhou, G. Hussain, Q. Li and K. Ostrikov, *Mater. Today Sustain.*, 2020, **10**, 100044.

12 P. B. Matad, P. B. Mokshanatha, N. Hebbar, V. T. Venkatesha and H. C. Tandon, *Ind. Eng. Chem. Res.*, 2014, **53**, 8436–8444.
13 M. Ben Harb, S. Abubshait, N. Etteyeb, M. Kamoun and A. Dhouib, *Arab. J. Chem.*, 2020, **13**, 4846–4856.
14 S. Rached, A. Habsaoui, K. Mzioud, R. Lachhab, S. Haida, N. Errahmany, M. Galai and M. E. Touhami, *Chem. Data Collect.*, 2023, **48**, 101099.
15 M. Abdallah, H. M. Altass, B. A. AL Jahdaly and M. M. Salem, *Green Chem. Lett. Rev.*, 2018, **11**, 189–196.
16 Z. Zhou, X. Min, S. Wan, J. Liu, B. Liao and X. Guo, *Results Eng.*, 2023, **17**, 100971.
17 D. Ben Hmamou, R. Salghi, L. Bazzi, B. Hammouti, S. S. Al-Deyab, L. Bammou, L. Bazzi and A. Bouyanzer, *Int. J. Electrochem. Sci.*, 2012, **7**, 1303–1318.
18 Q. Wang, X. Wu, H. Zheng, L. Liu, Q. Zhang, A. Zhang, Z. Yan, Y. Sun, Z. Li and X. Li, *J. Build. Eng.*, 2023, **63**, 105568.
19 R. Naderi, A. Bautista, F. Velasco, M. Soleimani and M. Pourfath, *J. Build. Eng.*, 2022, **58**, 105055.
20 K. Subbiah, H. S. Lee, S. Mandal and T. Park, *ACS Appl. Mater. Interfaces*, 2021, **13**, 43676–43695.
21 C. Liu, Y. Liu, Z. Xia, Z. Wang and B. Wu, *J. Build. Eng.*, 2024, **82**, 108194.
22 Y. Zarki, M. Elmourabit, N. Ben Seddik, S. Akachar, M. Achache, H. O. Idriss, F. Chaouket, K. Draoui and A. AitAghzzaf, *Surf. Interfaces*, 2024, **51**, 104754.
23 G. Vasyliev and V. Vorobiova, *Mater. Today Proc.*, 2019, **6**, 178–186.
24 P. B. Raja and M. G. Sethuraman, *Mater. Lett.*, 2008, **62**, 113–116.
25 B. Zakariae, *Université Sidi Mohamed Ben Abdellah*, Faculté des Sciences Dhar El Mahraz, 2018.
26 S. Z. Salleh, A. H. Yusoff, S. K. Zakaria, M. A. A. Taib, A. Abu Seman, M. N. Masri, M. Mohamad, S. Mamat, S. Ahmad Sobri, A. Ali and P. Ter Teo, *J. Cleaner Prod.*, 2021, **304**, 127030.
27 C. Venkatesh, S. K. Mohiddin and N. Ruben, in *Lecture Notes in Civil Engineering*, Springer, 2019, vol. 25, pp. 127–134.
28 M. A. Chowdhury, M. M. S. Ahmed, N. Hossain, M. A. Islam, S. Islam and M. M. Rana, *Results Eng.*, 2023, **17**, 100996.
29 S. A. Asipita, M. Ismail, M. Z. A. Majid, Z. A. Majid, C. Abdullah and J. Mirza, *J. Clean. Prod.*, 2014, **67**, 139–146.
30 S. P. Palanisamy, G. Maheswaran, A. G. Selvarani, C. Kamal and G. Venkatesh, *J. Build. Eng.*, 2018, **19**, 376–383.
31 S. A. Alshehri, S. Wahab, S. S. Abullais, G. Das, U. Hani, W. Ahmad, M. Amir, A. Ahmad, G. Kandasamy and R. Vasudevan, *Plants*, 2022, **11**, 118.
32 S. Lahbabi, R. Bouferra, L. Saadi and A. Khalil, *Constr. Build. Mater.*, 2024, **411**, 134304.
33 I. H. Ali, *Molecules*, 2021, **26**, 3679.
34 H. Gul, R. D. Naseer, I. Abbas, E. A. Khan, H. U. Rehman, A. Nawaz, A. K. Azad, G. M. Albadrani, A. E. Altyar, A. Albrakati and M. M. Abdel-Daim, *Medicina*, 2023, **59**, 34.
35 S. Said, G. Noureddine, L. S. Eddine, G. Abdelmadjid, B. Djamel and A. Tliba, *Res. J. Pharm. Technol.*, 2018, **11**, 3826–3832.
36 European Committee for Standardization (CEN), *EN 10025-2:2019 – Hot Rolled Products of Structural Steels – Part 2: Technical Delivery Conditions for Non-alloy Structural Steels*, Brussels, 2019.
37 R. Bahramsoltani, M. Kalkhorani, S. M. Abbas Zaidi, M. H. Farzaei and R. Rahimi, *J. Ethnopharmacol.*, 2020, **246**, 112245.
38 A. Mahfoudhi, F. P. Prencipe, Z. Mighri and F. Pellati, *J. Pharm. Biomed. Anal.*, 2014, **99**, 97–105.
39 R. Ksouri, H. Falleh, W. Megdiche, N. Trabelsi, B. Mhamdi, K. Chaieb, A. Bakrouf, C. Magné and C. Abdelly, *Food Chem. Toxicol.*, 2009, **47**, 2083–2091.
40 N. K. Upadhyay, M. S. Yogendra Kumar and A. Gupta, *Food Chem. Toxicol.*, 2010, **48**, 3443–3448.
41 I. H. Shah, M. Ashraf, A. R. Khan, M. A. Manzoor, K. Hayat, S. Arif, I. A. Sabir, M. Abdullah, Q. Niu and Y. Zhang, *3 Biotech*, 2022, **12**, 128.
42 M. Nasrollahzadeh, S. M. Sajadi and M. Maham, *RSC Adv.*, 2015, **5**, 40628–40635.
43 B. Liao, S. Ma, S. Zhang, X. Li, R. Quan, S. Wan and X. Guo, *Int. J. Biol. Macromol.*, 2023, **239**, 124358.
44 C. Younos, R. Soulimani, N. Seddiqi, O. Baburi and A. Dicko, *Phytothérapie*, 2005, **3**, 248–251.
45 D. Kumari, T. Madhujith and A. Chandrasekara, *Food Sci. Nutr.*, 2016, 1–13.
46 Y. Yamamoto, H. Nishihara and K. Aramaki, *Corrosion*, 1992, **48**, 641–648.
47 T. R. Ovari, A. M. V. Brânzanic, G. Katona, G. S. Szabó and L. M. Muresan, *Mater. Today Commun.*, 2025, **46**, 112739.
48 A. Chaouiki, M. Chafiq, A. H. Al-Moubaraki, M. Bakhouch, M. El Yazidi and Y. G. Ko, *Arab. J. Chem.*, 2022, **15**, 104323.
49 E. G. Juárez, V. Y. Mena-Cervantes, J. Vazquez-Arenas, G. P. Flores and R. Hernandez-Altamirano, *ACS Sustain. Chem. Eng.*, 2018, **6**, 17230–17238.
50 D. M. Jamil, H. S. Aljibori and A. Alamiery, *Results Chem.*, DOI: **10.1016/j.rechem.2025.102193**.
51 S. Chaouki, PhD thesis, Université Abou Bekr Belkaid, 2012.
52 P. Singh and P. N. Dave, *Sci. Total Environ.*, 2025, **975**, 179301.
53 L. Huang, H. J. Li and Y. C. Wu, *J. Environ. Manage.*, 2023, **335**, 117531.
54 M. HosseinpourRokni, R. Naderi, M. Soleimani, E. Kowsari and M. Pourfath, *Corros. Sci.*, 2023, **216**, 111100.
55 J. Zhang, F. Yang, Y. Dai, Y. Liu, Y. Yu and S. Wang, *Langmuir*, 2023, **39**, 18043–18051.
56 H. Lgaz, I. M. Chung, R. Salghi, I. H. Ali, A. Chaouiki, Y. El Aoufir and M. I. Khan, *Appl. Surf. Sci.*, 2019, **463**, 647–658.
57 P. Shathani, E. N. Ogunmuyiwa, O. P. Oladijo and B. A. Obadele, *Chem. Therm. Dyn. & Therm. Anal.*, 2025, **19**, 100197.
58 M. Rehioui, S. Abbout, B. Benzidia, H. Hammouch, H. Erramli, N. A. Daoud, N. Badrane and N. Hajjaji, *Heliyon*, 2021, **7**, e06674.
59 B. Elsener and U. Angst, in *Science and Technology of Concrete Admixtures*, Elsevier Inc., 2016, pp. 321–339.
60 S. Chakri, *Université Pierre et Marie Curie*, 2015.
61 Y. Du, G. Habert and C. Brumaud, *Constr Build Mater*, 2022, **323**, 126571.

62 H. Ejima, J. J. Richardson, K. Liang, J. P. Best, M. P. Van Koeverden, G. K. Such, J. Cui and F. Caruso, *Science*, 2013, **341**, 154–157.
63 N. Slabbert, in *Plant Polyphenols*, eds. R. W. Hemingway and P. E. Laks, Springer, Boston, MA, New York, 1992, vol. 59, pp. 421–436.
64 K. Khanbabaee and T. van Ree, *Nat. Prod. Rep.*, 2001, **18**, 641–649.
65 F. Bentiss, M. Lebrini and M. Lagrenée, *Corros. Sci.*, 2005, **47**, 2915–2931.
66 A. Fiala and Y. Mechehoud, *Sci. Technol.*, 2012, **35**, 23–30.
67 O. Hamdaoui, M. Ouchefoun and M. Zerdaoui, *Revue des Sciences de l'Eau*, 2000, 13, 47–54.
68 J. Eid, H. Takenouti, B. Ait and S. Taibi, *Corros. Sci.*, 2020, **168**, 108556.